Received 17 October 2017; revised 3 November 2017; accepted 6 November 2017. Date of publication 23 November 2017; date of current version 20 December 2017. The review of this paper was arranged by Editor C. Surya.

Digital Object Identifier 10.1109/JEDS.2017.2774509

Gold-Nanoparticle-Coated Ge MIS Photodiodes

HAO-TSE HSIAO[1], I-CHENG YAO[1], I-CHIH NI[2], SHIEN-DER TZENG[2], WEI-FAN LIN[1], BO-YU LIN[1], AND CHU-HSUAN LIN[1]

1 Department of Opto-Electronic Engineering, National Dong Hwa University, Hualien 97401, Taiwan
2 Department of Physics, National Dong Hwa University, Hualien 97401, Taiwan

CORRESPONDING AUTHOR: C.-H. Lin (e-mail: chlin0109@gms.ndhu.edu.tw)

This work was supported by the Ministry of Science and Technology, Taiwan, under Grant MOST 104-2221-E-259-030-MY3.

ABSTRACT Ge photodiodes with ultra-high responsivities have been demonstrated with gold nanoparticle assistance. The responsivity can reach a value of 37.7 A/W, which corresponds to a gain of 76. Such a high responsivity originates from the amassment of photo-generated holes in Ge under the boundary of gold nanoparticles, which reduces the barrier for electron tunneling from metal to the hole-amassment Ge ring areas. The depletion layer thinning due to hole amassment is not only proved by band diagram simulation but also confirmed by capacitance measurement.

INDEX TERMS Gold nanoparticle, Ge, photodiode, responsivity.

I. INTRODUCTION

Photodetectors have been broadly used in daily life applications, such as imaging [1], biological threat detection [2], and ambient light detection [3], and open up possibilities for optical interconnects [4], spectrometer-on-a-chip technology [5], retinal prosthesis [6], [7] *etc*. For a photodiode, the most common structure adopted by photodetectors, high responsivity and gain are desirable [8]. Many methods have been tried to increase the responsivity, such as new materials [9], antireflection [10], and nanoparticles [11]. Nanoparticles can increase the responsivity via surface plasmon coupling. For example, the responsivity of a Ge photodetector can be increased by 34% with coating gold nanoparticles (AuNPs) [12]. Ge photodiodes are suitable for visible and infrared detection. However, material cost of bulk Ge is an issue. In this study, we have found pronounced responsivity enhancement of bulk Ge metal-insulator-semiconductor (MIS) photodiodes with suitable AuNP distribution, which may be applied to thin-film Ge in the future to overcome the material cost and speed issues [13], [14].

II. EXPERIMENTAL

AuNPs prepared in this study was $\sim$ 30 nm [12]. DL-cysteine ($C_3H_7NO_2S$) or mercaptohexanoic acid with different carbon chain lengths was used to modify the surface of AuNPs. The agglomeration of AuNPs can be avoided with these modification molecules. The AuNPs were then deposited on (100) n-type Ge substrates (with a resistivity of 1-30 Ω-cm and a thickness of 525 μm) by centrifugal assembly method [15]. Before deposition, Ge were first pre-treated by 3-Aminonpropyl-trimethimethoxysilan (APTMS) to make the surface positively charged [15]. Fig. 1 (c) shows the distribution of our AuNPs modified by 8-mercaptooctanoic acid (MOA), and the coverage ratio is 27.5 %. Finally, an Al circular gate (radius of 0.0125 cm) and a surrounding C-shaped electrode were thermally evaporated at the same time with a thickness of 180 nm (Fig. 1 (a)). The C-shaped electrode owns an outer radius of 0.25 cm and an inner radius of 0.125 cm (The area exposed formed by the inner circle is $\sim$ 0.05 cm^2). The large area of the C-shaped electrode will result in a small contact resistance, which could display a quasi-ohmic behavior [16], [17]. Native oxidation in room air will lead to the formation of GeO_2 on Ge [18], [19]. The thickness of GeO_2 shown in Fig. 1 (b) is $\sim$ 4 nm. The GeO_2 (native oxide) is not removed, and the demonstrated structure is an MIS diode. For comparison, control diodes without AuNP deposition were also prepared, and these control samples were also subjected to APTMS pre-treatment to exclude APTMS's influence. We also prepared control samples without APTMS pre-treatment.

III. RESULTS AND DISCUSSION

The current-voltage (I-V) test was conducted by Agilent B1500A semiconductor analyzer (Fig. 1(a)). The measured I-V curves are shown in Fig. 2(a). The light is first generated

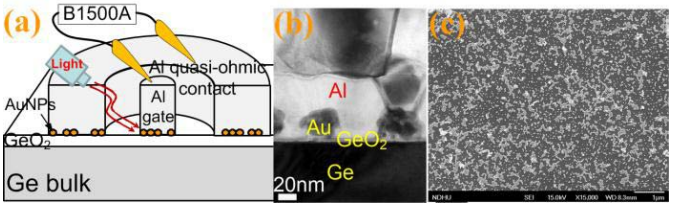

FIGURE 1. **(a) The schematic structure of an AuNP-coated Ge diode. (b) TEM photograph of the photodiode. (c) Distribution of AuNPs on Ge. The starting AuNP solution had a concentration of 4.6×10^{11} NPs/mL and a pH value of 4.25.**

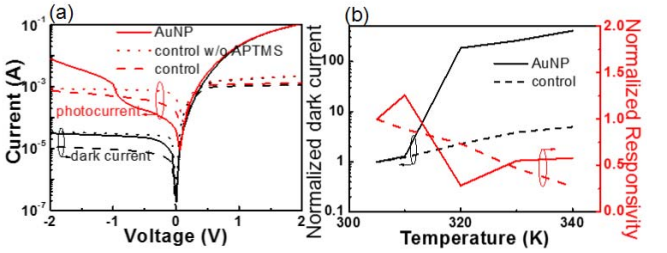

FIGURE 2. **(a) The I-V characteristics of AuNP, control, and control without APTMS diodes. (b) The temperature dependence of dark currents and responsivities at −2V. The values are normalized to their room-temperature values.**

from the laser diode, and then it is coupled into fiber. The core size of fiber is 9 μm. The wavelength of light is 1310 nm, and the output power from the fiber tip is 1.5 mW. The tip is close to the surface. The output of fiber tip irradiates by the edge of the Al gate at an incident angle of 45°. The position of fiber tip is fine-tuned until the maximum photocurrent is obtained. Once the fiber tip slightly moves towards the C-shaped electrode from the edge of the Al gate, the photocurrent decreases obviously because the photo-generated holes would have higher probability to recombine for the increased distance for diffusion. For a photodiode, the most important figure of merit is the responsivity (R), which is defined as (1),

$$R = \frac{photocurrent - dark\ current}{input\ optical\ power}\left(\frac{A}{W}\right) \tag{1}$$

At −2 V, the responsivity of AuNP, control, and control without APTMS diodes are 5.38, 0.498, and 0.552 A/W, respectively. AuNPs lead to obvious photocurrent jump at $-0.5 \sim -1$V, which results in the high responsivity as compared to other results [20], [21]. R is also given by (2) [22],

$$R = G\eta\frac{\lambda(\mu m)}{1.24} \tag{2}$$

where G is the gain (number of circuit carriers per photo-generated pairs); quantum efficiency (η) is the number of detectable photo-generated pairs produced per photon. When G of the control diode is considered as 1, its η would be 47 %. Since η is defined as pairs produced per photons, it is reasonable to suspect that η of the AuNP diode is $\sim$ 47 %, too. It can be deduced that gain of the AuNP diode is 10.9 from (2).

We then propose a model to explain the mechanism of photocurrent jump. The different work function (WF) between Au and Al leads to the amassment of photo-generated holes, and the subsequent depletion layer thinning lowers the barrier so that more electrons can flow from the gate to Ge by thermionic emission. The details are presented as follows.

The WF of Au (5.0 eV) is larger than that of Al (4.1 eV). When AuNPs are distributed in the Al gate electrode, their different WF will result in the different band bending of underlying Ge. At negative biases, valence band of Ge under Au would be higher than that of Al, and photo-generated holes prefer moving towards the GeO_2/Ge interface under Au instead of Al as schematic drawing in Fig. 3(a). In order to verify the supposed model, we simulated the band diagram using the simulation tool Sentaurus TCAD. Fig. 3(b) shows the simulated lateral Ge band diagram along the GeO_2/Ge interface when illuminated at −0.5 V. The inset of Fig. 3(b) shows the corresponding simulated AuNP structure. Photo-generated holes under Al prefer to move as indicated by the dash arrows in Fig. 3(b) in view of energy, and indicated by the solid arrows in the inset of Fig. 3(b) in view of real space. The −0.5 V band diagrams under (perpendicular to the GeO_2/Ge interface) AuNPs and other Al gate areas are also simulated as shown in Fig. 3(c) and Fig. 3(d), respectively. The curve "under Au_dark" depicts the band diagram under AuNPs of the AuNP diode without illumination; meanwhile, "under Au_photo" depicts the case with illumination. Photo-generated holes amass at the GeO_2/Ge interface, which results in depletion layer thinning (i.e., the depletion layer is thinned, and the top of E_c is also lowered). It should be noted that the amassment of photo-generated holes at the GeO_2/Ge interface locates at the ring areas projected by the upper Au/Al boundary. The lateral band diagram of Ge under Au are quite flat as shown in Fig. 3(b). Once the photo-generated holes under Al reach the ring under the Au/Al boundary, the vertical attraction will localize most holes here rather than moving to the center of the ring.

In the above simulation, the mechanism of tunneling is not considered. Poisson, electron continuity, and hole continuity equations are introduced in the device simulation. However, the stimulated AuNP structure with considering tunneling could not display current jump and depletion layer thinning behaviors. This is not consistent with the capacitance measurement discussed later. Therefore, we first studied the case where the tunneling mechanism is not considered, to analyze the effect of hole amassment. Then, the control diode with considering the tunneling mechanism is also simulated as shown in Fig. 3(e) for comparison. In Fig. 3(e), the unimpeded tunneling avoids the amassment of holes, and depletion layer thinning cannot be observed. Fig. 3(f) shows the enlarged view of E_c near the GeO_2/Ge interface of above three conditions. The lowering of E_c is obvious in simulated AuNP structures but not in the simulated control diode. The lowered E_c barrier for electron tunneling from gate to the Ge

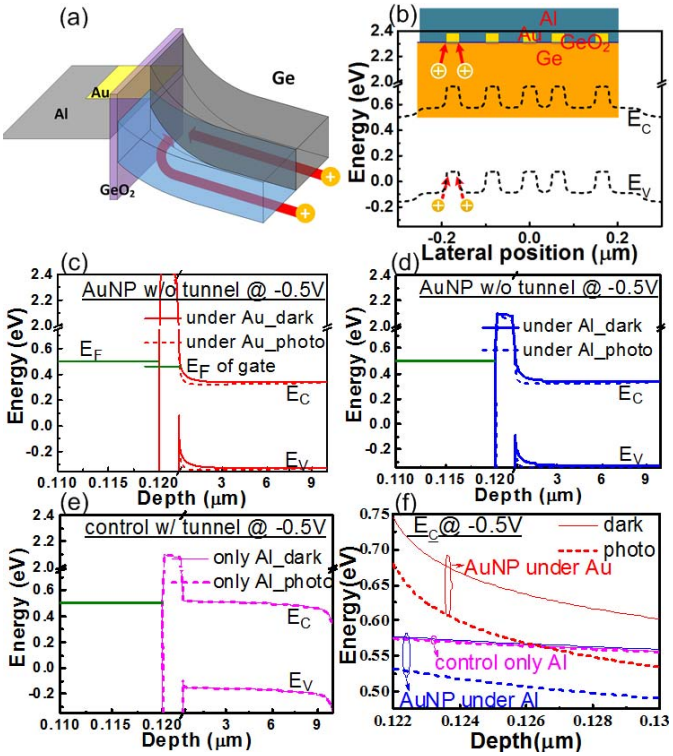

FIGURE 3. (a) The schematic model for hole amassment due to different band bending. (b) Lateral Ge band diagram along GeO_2/Ge interface when illuminated at −0.5 V. The inset shows the corresponding AuNP structure. −0.5 V diagrams underneath Au (c) and Al (d). (e) −0.5 V diagrams of the control diode with considering tunneling mechanism. (f) Enlarged view of E_C in (c), (d), and (e). Only 2-nm-thick GeO_2 is assumed to model the easily tunneling behavior of native GeO_2.

ring results in the extra electron flow in the practical AuNP diodes. This extra electron flow leads to the high gain of AuNP diodes while the gain of control diodes is 1 coming from the normal photocurrent contributed only by separation of photo-generated electron-hole pairs.

The bottleneck of the extra electron flow comes from the barrier formed by E_C of Ge rather than E_C of GeO_2 because the native GeO_2 is loose and easily tunneled. The thermionic emission flow for electrons overcoming the E_C barrier of Ge is given by (3) [16],

$$J_{m\to s} = A^* T^2 exp(\frac{-e\phi_{Bn}}{kT}) \tag{3}$$

where A^* is the effective Richardson constant, ϕ_{Bn} is electron barrier height. As shown in Fig. 3(f), the electron barrier from E_F of gate (at 0.5 eV) to top E_C of Ge of "AuNP under Al" without illumination (at 0.577 eV) is 0.077 eV; meanwhile the barrier from E_F of gate to top E_C of "AuNP under Al" with illumination is 0.032 eV. From (3), the ratio of $J_{m\to s}$ with illumination to $J_{m\to s}$ without illumination is 5.8. This large ratio indicates that illumination results in extra electron emission from the gate to Ge. The large slope of conduction band of Ge near the Ge/GeO_2 interface will let electrons keep moving without recombined with the amassed holes.

At lower negative biases, this lateral movement is detrimental for separation of photo-generated carriers. When holes spend more time in n-Ge due to the lateral movement and amassment, they will have more probability to recombine before collected by the gate. On the contrary, photo-generated holes in the control diode will be collected by the gate directly. Therefore, the responsivity of the AuNP diode is lower at the lower bias.

The sufficient thermal generated holes will also result in hole amassment. As temperature increasing to 320 K, the dark current of the AuNP diode significantly jumps and hence its responsivity decreases (Fig. 2(b)). In other temperature range, its responsivity increases as temperature increasing due to more thermionic emission from gate to Ge. On the other hand, dark currents of the control diode increase monotonically with temperature increasing, and hence its responsivities decrease monotonically (Fig. 2(b)).

As long as the distribution of AuNPs is uniform and density of AuNPS is large enough, devices with broad range of coverage ratios of AuNPs have all shown stable high gain. A gate only composed of single metal material (either Al or Au) will not have hole amassment and current jump phenomena. Photo-generated holes need to be temporarily amassed into a small area in order for the charge density buildup to outpace the loss of holes due to their tunneling into metal. If AuNPs are too sparse ("10.5% AuNPs" [12] for example), most photo-generated holes under Al would tunnel to Al directly and likewise cannot lead to the jump. If AuNPs are dense but agglomerated, the actual Au/Al boundary may not be long enough for jump behaviors (30.3% AuNPs" [12]). In [12], the AuNPs result in 34% enhancement on responsivity because the plasmonic interaction results in lower reflectance at interface. Such a mechanism could not result in a gain larger than 1. In this manuscript, the extra electron tunneling current result in the gain of 10. 9.

Fig. 4(a) shows the relation between light intensity and normalized capacitance, which corresponds to the ratio of capacitance (measured by Agilent E4980A at 1 MHz) with illumination to its capacitance without illumination. The normalized capacitance of the AuNP diode at −0.5 V is obviously larger than that of the control diode. This "AuNP @−0.5V" curve also reveals that larger light intensity leads to larger normalized capacitance, whereas the "control @−0.5V" curve is much less sensitive to light intensity. This proves that hole amassment only occurs in the AuNP diode. The change of depletion width can only be easily observed before tunneling dominates; so we chose the −0.5 V for capacitance measurement. At 0 V, far fewer photo-generated holes could be collected to the GeO_2/Ge interface, and hence the obvious increase of capacitance due to depletion layer thinning cannot be observed.

The lower illumination intensity results in the obviously larger responsivity for the AuNP sample at −2 V (Fig. 4 (b)). The 0.1 mW of light can provide sufficient hole amassment under Au/Al boundary, and leads to the extra electron flow from metal to Ge at −2 V. The responsivity can reach a value

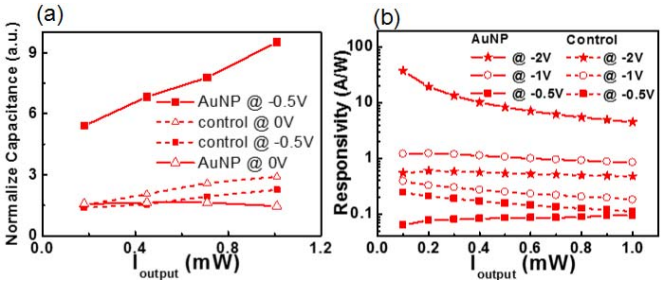

FIGURE 4. (a) Relation between light intensity and normalized capacitance. I_{output} is the output power from the fiber tip, and larger power corresponds to larger light intensity coupled into Ge. (b) Responsivity as a function of light intensity.

of 37. 7 A/W, which corresponds to a gain of 76. We have reached the high gain at −2 V, which is much smaller than the common bias of the avalanche photodiodes [4], [21]. The high responsivity at low illumination is beneficial to digital applications, such as optical interconnects, even with the nonlinear behaviors since only two states of "0" and "1" should be distinguished. Smaller input power would be needed for the "1" state. On the other hand, the nonlinearity indeed brings troubles to analog applications [23], [24]. The strong nonlinearity of AuNP sample at −2 V makes the readout current hard to be analyzed. For analog applications, such as imaging and spectrometer, the AuNP sample would be better to be operated at −1 V since the curve is much linear and owns larger responsivities as compared with control samples.

IV. CONCLUSION

We have demonstrated Ge photodiodes with ultra-high responsivities with the assistance of AuNPs. The different work function between Au and Al results in different band bending of underlying Ge. Photo-generated holes will amass under the Au/Al boundary, and it leads to the depletion layer thinning and the lowered barrier for extra electron-tunneling flow. Further investigation could be performed to demonstrate a high responsivity-bandwidth product on thin-film Ge in the future.

ACKNOWLEDGMENT

The authors are grateful to the National Center for High performance computing for computer time and facilities.

REFERENCES

[1] N. Guo *et al.*, "High-quality infrared imaging with graphene photodetectors at room temperature," *Nanoscale*, vol. 8, no. 35, pp. 16065–16072, Sep. 2016, doi: 10.1039/c6nr04607j.

[2] J. Wang, C. Yan, M.-F. Lin, K. Tsukagoshib, and P. S. Lee, "Solution-assembled nanowires for high performance flexible and transparent solar-blind photodetectors," *J. Mater. Chem. C*, vol. 3, no. 3, pp. 596–600, Jan. 2015, doi: 10.1039/c4tc02297a.

[3] A. Radoi, M. Dragoman, and D. Dragoman, "Plasmonic ambient light sensing with MoS2-graphene heterostructures," *Phys. E Low Dimensional Syst. Nanostruct.*, vol. 85, pp. 164–168, Jan. 2017, doi: 10.1016/j.physe.2016.08.026.

[4] K. Xu *et al.*, "Light emitting devices in Si CMOS and RF bipolar integrated circuits," *J. Illuminating Eng. Soc.*, vol. 12, no. 4, pp. 203–212, Oct. 2016, doi: 10.1080/15502724.2015.1134333.

[5] I. J. Luxmoore, P. Q. Liu, P. Li, J. Faist, and G. R. Nash, "Graphene-metamaterial photodetectors for integrated infrared sensing," *ACS Photon.*, vol. 3, no. 6, pp. 936–941, May 2016, doi: 10.1021/acsphotonics.6b00226.

[6] H. Lorach *et al.*, "Photovoltaic restoration of sight with high visual acuity," *Nat. Med.*, vol. 21, no. 5, pp. 476–482, Apr. 2015, doi: 10.1038/nm.3851.

[7] S. Ha *et al.*, "Towards high-resolution retinal prostheses with direct optical addressing and inductive telemetry," *J. Neural Eng.*, vol. 13, no. 5, Aug. 2016, Art. no. 056008, doi: 10.1088/1741-2560/13/5/056008.

[8] Y. Dong *et al.*, "Germanium–Tin on Si avalanche photodiode: Device design and technology demonstration," *IEEE Trans. Electron Devices*, vol. 62, no. 1, pp. 128–135, Jan. 2015, doi: 10.1109/TED.2014.2366205.

[9] T. N. Pham *et al.*, "Si-based $Ge_{0.9}Sn_{0.1}$ photodetector with peak responsivity of 2.85 A/W and longwave cutoff at 2.4 μm," *Electron. Lett.*, vol. 51, no. 11, pp. 854–856, May 2015, doi: 10.1049/el.2015.0331.

[10] H. So and D. G. Senesky, "ZnO nanorod arrays and direct wire bonding on GaN surfaces for rapid fabrication of antireflective, high-temperature ultraviolet sensors," *Appl. Surf. Sci.*, vol. 387, pp. 280–284, Nov. 2016, doi: 10.1016/j.apsusc.2016.05.166.

[11] K. Hu *et al.*, "Broadband photoresponse enhancement of a high-performance t-Se microtube photodetector by plasmonic metallic nanoparticles," *Adv. Funct. Mater.*, vol. 26, no. 36, pp. 6641–6648, Sep. 2016, doi: 10.1002/adfm.201602408.

[12] H.-T. Hsiao, I.-C. Ni, S.-D. Tzeng, W.-F. Lin, and C.-H. Lin, "The n-type Ge photodetectors with gold nanoparticles deposited to enhance the responsivity," *Nanoscale Res. Lett.*, vol. 9, no. 1, p. 640, Nov. 2014, doi: 10.1186/1556-276X-9-640.

[13] M. M. P. Fard, G. Cowan, and O. Liboiron-Ladouceur, "Responsivity optimization of a high-speed germanium-on-silicon photodetector," *Opt. Exp.*, vol. 24, no. 24, pp. 27738–27752, Nov. 2016, doi: 10.1364/OE.24.027738.

[14] I. A. Fischer *et al.*, "Ge-on-Si PIN-photodetectors with Al nanoantennas: The effect of nanoantenna size on light scattering into waveguide modes," *Appl. Phys. Lett.*, vol. 108, no. 7, Feb. 2016, Art. no. 071108, doi: 10.1063/1.4942393.

[15] I.-C. Ni *et al.*, "Formation mechanism, patterning, and physical properties of gold-nanoparticle films assembled by an interaction-controlled centrifugal method," *J. Phys. Chem. C*, vol. 116, no. 14, pp. 8095–8101, Mar. 2012, doi: 10.1021/jp211126v.

[16] S. M. Sze and K. K. Ng, *Physics of Semiconductor Devices*, 3rd ed. Hoboken, NJ, USA: Wiley, 2007.

[17] V. Venkatesan *et al.*, "Effect of thin interfacial SiO_2 films on metal contacts to B-doped diamond films," *J. Electrochem. Soc.*, vol. 139, no. 5, pp. 1445–1449, May 1992, doi: 10.1149/1.2069428.

[18] S. K. Sahari *et al.*, "Native oxidation growth on Ge(111) and (100) surfaces," *Jpn. J. Appl. Phys.*, vol. 50, no. 4, Apr. 2011, Art. no. 04DA12, doi: 10.1143/JJAP.50.04DA12.

[19] T. Deegan and G. Hughes, "An X-ray photoelectron spectroscopy study of the HF etching of native oxides on Ge(111) and Ge(100) surfaces," *Appl. Surf. Sci.*, vols. 123–124, pp. 66–70, Jan. 1998, doi: 10.1016/S0169-4332(97)00511-4.

[20] M. Morse *et al.*, "Performance of Ge/Si receivers at 1310 nm," *Phys. E Low Dimensional Syst. Nanostruct.*, vol. 41, no. 6, pp. 1076–1081, May 2009, doi: 10.1016/j.physe.2008.08.017.

[21] A. Sammak, M. Aminian, L. K. Nanver, and E. Charbon, "CMOS-compatible pureGaB Ge-on-Si APD pixel arrays," *IEEE Trans. Electron Devices*, vol. 63, no. 1, pp. 92–99, Jan. 2016, doi: 10.1109/TED.2015.2457241.

[22] B. E. A. Saleh and M. C. Teich, *Fundamentals of Photonics*. New York, NY, USA: Wiley, 1991, p. 651.

[23] K. Rahmelow, "Electronic influences on an infrared detector signal: Nonlinearity and amplification," *Appl. Opt.*, vol. 36, no. 10, pp. 2123–2132, Apr. 1997, doi: 10.1364/AO.36.002123.

[24] E. I. Ackerman and C. H. Cox, "RF fiber-optic link performance," *IEEE Microw. Mag.*, vol. 2, no. 4, pp. 50–58, Dec. 2001, doi: 10.1109/6668.969935.

HAO-TSE HSIAO received the B.S. degree from the Department of Physics, National Dong Hwa University, Taiwan, in 2012 and the M.S. degree from the Department of Opto-Electronic Engineering, National Dong Hwa University, in 2014.

I-CHENG YAO was born in Taiwan in 1991. He received the M.S. degree from the Department of Opto-Electronic Engineering, National Dong Hwa University, Taiwan. He is currently a Technology Development Engineer with Episil Technologies Inc.

I-CHIH NI received the Ph.D. degree from the Department of Physics, National Dong Hwa University, Hualien, Taiwan, in 2017. He is currently a Post-Doctoral Fellow with the Institute of Photonics and Optoelectronics, National Taiwan University, Taipei, Taiwan. His research interests center on self-assembled nanoparticles films, SAM-nanoparticle devices, and flexible electron device.

SHIEN-DER TZENG was born in Taiwan, in 1974. He received the B.S. and Ph.D. degrees from the Department of Physics, National Tsing Hwa University, Taiwan, in 1996 and 2006, respectively. He is currently an Associate Professor with the Department of Physics, National Dong Hwa University, Hualien, Taiwan. His research interest center on assembly of nano-materials and their properties.

WEI-FAN LIN was born in Taiwan, in 1991. He received the master's degree from the Department of Opto-Electronic Engineering, National Dong Hwa University, Hualien, Taiwan, in 2015. He is currently a Senior Engineer with Macronix International Company Ltd., Hsinchu, Taiwan. His main job in MXIC is developing and testing the embedded multimedia card.

BO-YU LIN was born in Taiwan, in 1994. He received the B.E. degree from the Department of Opto-Electronic Engineering, National Dong Hwa University, Taiwan, in 2016, where he is currently pursuing the M.S. degree.

CHU-HSUAN LIN was born in Taiwan. He received the B.E. degree from the Department of Electronics Engineering, National Chiao Tung University, Taiwan, and the Ph.D. degree from the Department of Electrical Engineering and Graduate Institute of Electronics Engineering, National Taiwan University, Taiwan, in 2008. He is currently a Professor with the Department of Opto-Electronic Engineering, National Dong Hwa University, Hualien, Taiwan. His research interests center on solar cells, photodetectors, and applications on optical energy conversion based on graphene oxide.